

## The effect of the hedenbergitic substitution on the compressibility of jadeite

F. NESTOLA,<sup>1,2,\*</sup> T. BOFFA BALLARAN,<sup>1</sup> C. LIEBSKE,<sup>3,†</sup> R. THOMPSON,<sup>4</sup> AND R.T. DOWNS<sup>4</sup>

<sup>1</sup>Bayerisches Geoinstitut, Universität Bayreuth, Universitätsstrasse 30, D-95447 Bayreuth, Germany

<sup>2</sup>Dipartimento di Geoscienze, Università di Padova, Via Giotto 1, I-35137 Padova, Italy

<sup>3</sup>Institute for Mineralogy and Petrology, ETH Zurich, Clausiusstrasse 25, CH-8092, Zurich, Switzerland

<sup>4</sup>Department of Geosciences, University of Arizona, Tuscon, Arizona, 85721-0077, U.S.A.

### ABSTRACT

Four synthetic crystals belonging to the jadeite (Jd, NaAlSi<sub>2</sub>O<sub>6</sub>)-hedenbergite (Hd, CaFeSi<sub>2</sub>O<sub>6</sub>) solid solution were investigated by X-ray diffraction in situ at high pressure using a diamond anvil cell to  $P_{\max} = 10.6$  GPa. The samples exhibited space group symmetry  $C2/c$  throughout the investigated pressure range and did not show any phase transformations.  $V_0$ ,  $K_{T0}$ , and  $K'$  were simultaneously refined by fitting a third-order Birch-Murnaghan equation of state to pressure-volume data for all samples. The following relationship between bulk modulus and molar fraction of jadeite is observed:

$$K_{T0} = 108.7(2) \text{ (GPa)} + 0.191(9) \times [\% \text{ molar Jd}] + 0.0006(1) \times [\% \text{ molar Jd}]^2$$

The bulk modulus of hedenbergite is 19% lower than jadeite with a strong axial anisotropy that increases with increasing the Hd content. In particular, the compressibility along the **b** axis (the most compressible in pyroxenes) increases by about 35% going from Jd to Hd while along the **c** axis the increase in compressibility is about 24%. The **a** axis does not show any variation in the deformation rate along the join. The analysis of the crystal structure behavior with pressure for all samples clearly indicates that the main cause of the strong anisotropy on the **b-c** plane is related to the narrowing of the M1 octahedral chain and to anion-anion interactions increasing the packing efficiency of the anion skeletons of the crystals going from Jd to Hd.

**Keywords:** High pressure, solid solution, crystal structure, X-ray

### INTRODUCTION

Due to their significant abundance in the Earth's lower crust and upper mantle, clinopyroxenes have been the subject of several investigations at high pressure (e.g., Hugh-Jones and Angel 1994; Hugh-Jones et al. 1997; Tribaudino et al. 2001; Thompson and Downs 2004, 2007; Nestola et al. 2004, 2005; Thompson et al. 2005; Downs and Singh 2006; McCarthy et al. 2007).

In particular, studies at high pressure have demonstrated that Mg-pyroxenes and Na-pyroxenes can be stable over a wide range of pressures and temperatures. In particular, jadeite (Jd, NaAlSi<sub>2</sub>O<sub>6</sub>) is a significant component in pyroxenes in metamorphosed crust (see, e.g., Holland 1983). Therefore, studying Na-clinopyroxenes provides fundamental information on the geological environment in this region of the Earth. Some investigations have been performed on jadeite-diopside (Di, CaMgSi<sub>2</sub>O<sub>6</sub>) and jadeite-aegirine (Ae, NaFeSi<sub>2</sub>O<sub>6</sub>) solid solutions (Pavese et al. 2001; Nestola et al. 2006; McCarthy et al. 2007) to determine the high-pressure behavior and compressibility ( $\beta$ ) of Na-clinopyroxenes characterized by the most

common substitutions occurring in natural samples. In Pavese et al. (2001) and Nestola et al. (2006), the compressibility  $\beta$  of jadeite was determined as a function of diopside and aegirine component and in both studies the decrease of Jd component is correlated with a significant increase in compressibility. Jadeite also forms a third important solid solution with hedenbergite (Hd, CaFeSi<sub>2</sub>O<sub>6</sub>). However, there are no data at high pressure for the jadeite-hedenbergite solid solution and only one study of end-member hedenbergite at pressure (Zhang et al. 1997).

The aim of this work is to determine how the bulk modulus  $K_{T0} = -1/\beta$  changes as a function of composition along the jadeite-hedenbergite join, in order to complete the catalog of compressibilities of Na-clinopyroxenes for common natural compositions and to further our understanding of pyroxene crystal structure behavior under pressure. This study has been carried out on four single-crystals belonging to the Jd-Hd solid solution synthesized at high-pressure and high-temperature conditions in a multi-anvil press. The samples have been investigated by in-situ single-crystal X-ray diffraction at high pressure using a diamond anvil cell.

### EXPERIMENTAL METHODS

The crystal of jadeite studied here is the same sample used by Nestola et al. (2006) in an investigation performed at high pressure along the jadeite-aegirine solid solution, in which the authors determined the unit-cell parameters with pres-

\* E-mail: fabrizio.nestola@unipd.it

† Present address: Corus RD and T, Ceramics Research Centre, 1970 CA Ijmuiden, The Netherlands.

sure. Nestola et al. (2006), however, did not report crystal structure data. Here, therefore, the crystal structure evolution of jadeite has been determined up to 8.3 GPa. Other samples along the jadeite-hedenbergite solid solution were previously studied by Nestola et al. (2007), who investigated them by single-crystal X-ray diffraction under ambient conditions. They have the following compositions:  $\text{Jd}_{53}\text{Hd}_{47}$ ,  $\text{Jd}_{24}\text{Hd}_{76}$ , and  $\text{Jd}_0\text{Hd}_{100}$ . Synthesis conditions, crystal size and quality, and crystal-structure data can be found in Nestola et al. (2007).

High-pressure diffraction experiments were performed with a BGI design diamond-anvil cell (BGI-DAC, Allan et al. 1996), using steel gaskets (T301) pre-pressed to a thickness ranging between 100 and 80  $\mu\text{m}$  and holes with diameters between 300 and 250  $\mu\text{m}$ . Single crystals of quartz were used as internal diffraction pressure standards (Angel et al. 1997) and a mixture of methanol:ethanol:water with ratios of 16:3:1 was used as hydrostatic pressure medium. Unit-cell parameters at different pressures were determined for all the hedenbergite samples using the same experimental procedures outlined in Nestola et al. (2006), reported in Table 1.

Intensity data were collected at high pressure for all samples using a Kappa geometry Xcalibur diffractometer with graphite monochromated  $\text{MoK}\alpha$  up to  $2\theta_{\text{max}} \leq 60^\circ$  in  $\omega$ -scan mode with a continuous integrative step scan (0.05°/s, 60 scan steps, scan width 1.2°) using a point-detector. The sample-detector distance was 135 mm. The program Win-IntegrStp (version 3.3, Angel 2003) was used to integrate the step-scan data applying the Lorentz-polarization correction. The intensity data were corrected for absorption using the program ABSORB V6.0 (Angel 2004). Weighted structural isotropic refinements were done at all pressures and for all samples using the SHELX-97 package (Sheldrick 1997) starting from the atomic coordinates of Nestola et al. (2007). The atomic scattering curves were taken from the *International Tables for X-ray Crystallography* (Ibers and Hamilton 1974). The occupancies for the intermediate compositions were fixed to the values obtained by Nestola et al. (2007) since, as above described, exactly the same crystals were used in this work. The atomic coordinates and isotropic displacement parameters are reported in Table 2, whereas the bond lengths, polyhedral volumes, the distortion parameter  $\Delta\text{M}^2$ , quadratic elongation, angle variance, and kinking angle are reported in Table 3. All the high-pressure experiments were performed at the single-crystal diffraction laboratory at the Bayerisches Geoinstitut.

## RESULTS

### Bulk modulus $K_{\text{T}0}$ as a function of composition along the jadeite-hedenbergite join

The evolution of the unit-cell parameters as well as that of the unit-cell volumes of all samples as a function of pressure is shown in Figure 1. It is evident that no phase transitions were found in the pressure range investigated. Figure 1 illustrates that the unit-cell parameters for jadeite [Nestola et al. (2006) reported in the figure for purpose of comparison] decrease nearly linearly with pressure, but as the Hd content increases, the variations in unit-cell parameters show a strong curvature and an increase in the axial compressional anisotropy. The plots of the  $\beta$  angle and unit-cell volume vs. pressure show similar behavior, increasing their curvature at high pressure with increasing Hd content.

The pressure-volume data for all samples were fit with a third-order Birch-Murnaghan equation of state (BM3; Birch 1947) and the fitting results are reported in Table 4. The fit was performed using EoS-FIT5.2 program (Angel 2002) and three BM3 coefficients (unit-cell volume  $V_0$ , bulk modulus  $K_{\text{T}0}$  and its first pressure derivative  $K'$ ) were refined simultaneously for all compositions. The bulk modulus  $K_{\text{T}0}$  decreases with increasing Hd content, and for end-member jadeite and hedenbergite the difference is about 19%. The evolution of  $K_{\text{T}0}$  as a function of percent molar jadeite content is reported in Figure 2. In this figure, it is evident that the change in  $K_{\text{T}0}$  is not linear and the  $K_{\text{T}0}$ -composition data can be fitted by a weighted second order polynomial as follows:

$$K_{\text{T}0} = 108.7(2) \text{ (GPa)} + 0.191(9) \times [\% \text{ molar Jd}] + 0.0006(1) \times [\% \text{ molar Jd}]^2 \quad (1)$$

**TABLE 1.** Unit-cell parameters vs. pressure measured along the join jadeite-hedenbergite studied in this work

$P$ (GPa)	$a$ (Å)	$b$ (Å)	$c$ (Å)	$\beta$ (°)	$V$ (Å <sup>3</sup> )
<b>Jd<sub>53</sub>Hd<sub>47</sub></b>					
0.00010(1)	9.6031(3)	8.7735(3)	5.2656(2)	106.725(3)	424.88(2)
0.069(5)	9.6013(6)	8.7721(6)	5.2643(4)	106.712(5)	424.65(5)
0.150(4)	9.5993(2)	8.7692(3)	5.2636(2)	106.708(2)	424.38(2)
0.342(4)	9.5938(5)	8.7639(6)	5.2605(4)	106.679(5)	423.69(4)
0.750(6)	9.5824(4)	8.7535(4)	5.2550(2)	106.629(3)	422.35(2)
1.145(4)	9.5730(3)	8.7416(3)	5.2495(2)	106.586(3)	421.01(2)
1.569(4)	9.5618(3)	8.7304(3)	5.2436(2)	106.535(3)	419.62(3)
1.968(4)	9.5522(3)	8.7190(3)	5.2380(2)	106.491(2)	418.30(2)
2.686(6)	9.5352(3)	8.7004(3)	5.2284(2)	106.417(3)	416.09(2)
3.200(5)	9.5235(3)	8.6872(3)	5.2214(2)	106.365(3)	414.48(2)
3.652(6)	9.5135(3)	8.6765(3)	5.2158(2)	106.317(3)	413.20(2)
4.603(6)	9.4926(3)	8.6525(3)	5.2038(2)	106.227(3)	410.38(2)
5.401(6)	9.4761(3)	8.6329(3)	5.1940(2)	106.158(3)	408.12(2)
6.091(6)	9.4632(3)	8.6170(3)	5.1857(2)	106.097(3)	406.29(2)
6.707(7)	9.4516(3)	8.6027(2)	5.1784(2)	106.044(2)	404.65(2)
7.212(7)	9.4427(3)	8.5916(3)	5.1727(2)	106.008(3)	403.38(2)
7.468(7)	9.4377(3)	8.5861(3)	5.1700(2)	105.988(3)	402.73(2)
7.713(7)	9.4336(5)	8.5807(7)	5.1674(4)	105.964(5)	402.15(5)
8.058(9)	9.4295(3)	8.5718(5)	5.1634(2)	105.937(2)	401.30(2)
<b>Jd<sub>24</sub>Hd<sub>76</sub></b>					
0.00010(1)	9.7340(2)	8.9103(4)	5.2682(2)	105.904(2)	439.44(3)
0.841(5)	9.7116(2)	8.8831(4)	5.2553(2)	105.775(2)	436.30(3)
1.182(5)	9.7032(2)	8.8723(4)	5.2500(2)	105.725(2)	435.06(3)
1.882(5)	9.6856(1)	8.8509(3)	5.2398(1)	105.630(2)	432.58(2)
2.229(5)	9.6773(1)	8.8400(3)	5.2348(1)	105.583(1)	431.37(2)
3.045(5)	9.6590(1)	8.8160(4)	5.2235(2)	105.484(2)	428.66(2)
3.867(7)	9.6410(1)	8.7920(3)	5.2122(1)	105.391(1)	425.96(2)
4.985(8)	9.6185(2)	8.7614(5)	5.1981(2)	105.282(2)	422.57(3)
6.768(9)	9.5852(2)	8.7143(4)	5.1769(2)	105.121(2)	417.44(2)
8.764(8)	9.5525(2)	8.6648(5)	5.1550(2)	104.972(3)	412.20(3)
10.620(11)	9.5252(3)	8.6200(7)	5.1360(3)	104.854(3)	407.61(4)
9.827(9)*	9.5373(3)	8.6385(6)	5.1441(2)	104.907(3)	409.50(4)
<b>Jd<sub>0</sub>Hd<sub>100</sub></b>					
0.00010(1)	9.8447(2)	9.0234(3)	5.2509(2)	104.862(2)	450.84(2)
0.539(5)	9.8300(2)	9.0050(2)	5.2412(2)	104.756(2)	448.65(2)
1.038(4)	9.8165(2)	8.9879(3)	5.2331(2)	104.670(2)	446.66(2)
1.673(4)	9.8006(3)	8.9676(3)	5.2230(2)	104.573(2)	444.27(2)
2.294(5)	9.7874(3)	8.9465(3)	5.2139(2)	104.475(2)	442.05(2)
3.134(5)	9.7687(6)	8.9201(7)	5.2018(5)	104.371(6)	439.09(5)
3.800(5)	9.7553(4)	8.8998(4)	5.1923(3)	104.290(3)	436.84(3)
5.528(7)	9.7221(4)	8.8501(4)	5.1708(3)	104.127(3)	431.44(3)
7.000(7)	9.6972(5)	8.8099(6)	5.1538(4)	104.013(5)	427.19(4)
7.786(7)	9.6848(3)	8.7889(3)	5.1451(2)	103.961(3)	425.00(2)

Note: One standard deviation is reported in parentheses.

\* Data measured during decompression.

The first pressure derivative  $K'$  is not constant along the join and increases significantly with increasing Hd content. In particular, it shows a value of 4.4(1) for pure jadeite (Nestola et al. 2006) and increases linearly to 6.6(1) for pure hedenbergite. This is visible in the  $F_E$ - $f_E$  plot, where  $F_E$  is the "normalized pressure"  $F_E = P/3 \times f_E \times (1 + 2f_E)^{5/2}$  and  $f_E$  is the "normalized strain"  $f_E = [(V_0/V)^{2/3} - 1]/2$  (for details see Angel 2000), illustrated in Figure 3 for all samples. The linear regressions indicated by solid lines in Figure 3 clearly demonstrated that  $K_{\text{T}0}$  (=intercept) decreases while  $K' [= (2 \times \text{slope} + 12 K_{\text{T}0})/3K_{\text{T}0}]$  increases with increasing Hd content along the Jd-Hd join.

### Axial compressibilities

To determine the axial modulus for  $a$ ,  $b$ , and  $c$ , we used a parameterized form of the BM3 implemented in the EoS-FIT5.2 program in which the individual axes are cubed. The equation of state coefficients for all samples are reported in Table 4. The relative axial compressibility calculated using the relation for

**TABLE 2.** Atomic coordinates and isotropic thermal parameters for the samples studied in this work ( $U_{\text{iso}}$  is given in  $\text{\AA}^2$ )

		<b>Jd<sub>100</sub>Hd<sub>0</sub></b>			<b>Jd<sub>53</sub>Hd<sub>47</sub></b>		
		0 GPa	3.14 GPa	8.31 GPa	0 GPa	3.65 GPa	6.09 GPa
M2	x	0	0	0	0	0	0
	y	0.3002(2)	0.3019(6)	0.3041(5)	0.3008(2)	0.3024(5)	0.3046(7)
	z	0.25	0.25	0.25	0.25	0.25	0.25
	$U_{\text{iso}}$	0.0086(4)	0.0110(9)	0.0091(9)	0.0133(6)	0.011(1)	0.012(1)
M1	x	0	0	0	0	0	0
	y	0.9061(1)	0.9076(4)	0.9082(4)	0.9050(1)	0.9061(4)	0.9066(5)
	z	0.25	0.25	0.25	0.25	0.25	0.25
	$U_{\text{iso}}$	0.0049(3)	0.0059(6)	0.0053(6)	0.0079(4)	0.0087(7)	0.0068(8)
T	x	0.2902(3)	0.2905(2)	0.2908(3)	0.2883(5)	0.2886(3)	0.2888(4)
	y	0.0935(1)	0.0941(3)	0.0949(2)	0.0922(1)	0.0920(4)	0.0928(5)
	z	0.2281(2)	0.2288(3)	0.2294(3)	0.2298(2)	0.2301(4)	0.2300(5)
	$U_{\text{iso}}$	0.0045(3)	0.0050(5)	0.0055(5)	0.0078(4)	0.0068(7)	0.0074(8)
O1	x	0.1112(8)	0.1090(6)	0.1093(6)	0.1122(7)	0.1145(9)	0.1125(9)
	y	0.0757(2)	0.0782(7)	0.0784(6)	0.0802(4)	0.0817(11)	0.0825(13)
	z	0.1293(4)	0.1291(8)	0.1309(8)	0.1365(8)	0.1369(12)	0.1366(14)
	$U_{\text{iso}}$	0.0056(4)	0.006(1)	0.0046(9)	0.0189(9)	0.015(2)	0.014(2)
O2	x	0.3602(7)	0.3603(6)	0.3596(7)	0.3593(10)	0.3591(9)	0.3588(11)
	y	0.2634(2)	0.2652(6)	0.2674(6)	0.2556(4)	0.2571(10)	0.2589(11)
	z	0.2939(4)	0.2976(8)	0.3027(9)	0.3088(7)	0.3093(13)	0.3124(14)
	$U_{\text{iso}}$	0.0072(4)	0.007(1)	0.008(1)	0.0112(8)	0.013(2)	0.012(2)
O3	x	0.3534(6)	0.3555(6)	0.3566(7)	0.3525(10)	0.3529(9)	0.3544(11)
	y	0.0071(2)	0.0099(6)	0.0146(6)	0.0128(4)	0.0166(9)	0.0188(11)
	z	1.0066(4)	1.0052(8)	1.0009(9)	1.0011(6)	0.9982(13)	0.9967(16)
	$U_{\text{iso}}$	0.0075(4)	0.008(1)	0.007(1)	0.0113(8)	0.009(1)	0.011(2)
		<b>Jd<sub>24</sub>Hd<sub>76</sub></b>			<b>Jd<sub>0</sub>Hd<sub>100</sub></b>		
		0 GPa	3.87 GPa	8.76 GPa	0 GPa	3.80 GPa	
M2	x	0	0	0	0	0	
	y	0.3006(2)	0.3019(10)	0.305(1)	0.3001(1)	0.3021(2)	
	z	0.25	0.25	0.25	0.25	0.25	
	$U_{\text{iso}}$	0.0095(4)	0.012(1)	0.012(2)	0.0083(2)	0.0096(5)	
M1	x	0	0	0	0	0	
	y	0.9059(1)	0.9056(7)	0.908(1)	0.90740(7)	0.9086(2)	
	z	0.25	0.25	0.25	0.25	0.25	
	$U_{\text{iso}}$	0.0077(3)	0.0061(8)	0.007(1)	0.0065(2)	0.0086(4)	
T	x	0.2883(5)	0.2885(2)	0.2883(3)	0.2877(4)	0.2878(2)	
	y	0.0920(1)	0.0927(5)	0.0946(9)	0.09253(9)	0.0936(2)	
	z	0.2315(2)	0.2317(4)	0.2309(6)	0.2325(2)	0.2314(3)	
	$U_{\text{iso}}$	0.0077(3)	0.010(1)	0.012(1)	0.0052(3)	0.0061(4)	
O1	x	0.1146(7)	0.1167(4)	0.1155(6)	0.1193(8)	0.1201(5)	
	y	0.0855(4)	0.086(1)	0.089(2)	0.0907(2)	0.0911(6)	
	z	0.1454(7)	0.1482(9)	0.146(1)	0.1522(5)	0.1522(8)	
	$U_{\text{iso}}$	0.0163(8)	0.014(2)	0.014(2)	0.0083(6)	0.0092(9)	
O2	x	0.3610(9)	0.3602(7)	0.359(1)	0.3624(8)	0.3621(6)	
	y	0.2508(3)	0.2539(5)	0.2583(9)	0.2464(3)	0.2496(6)	
	z	0.3167(6)	0.320(1)	0.323(2)	0.3245(5)	0.3262(8)	
	$U_{\text{iso}}$	0.0107(7)	0.019(2)	0.021(3)	0.0089(6)	0.013(1)	
O3	x	0.3496(9)	0.3540(5)	0.3550(8)	0.3502(8)	0.3519(5)	
	y	0.0158(4)	0.0200(7)	0.023(1)	0.0195(3)	0.0226(6)	
	z	0.9987(6)	0.9946(10)	0.989(1)	0.9938(4)	0.9885(8)	
	$U_{\text{iso}}$	0.0108(8)	0.008(2)	0.011(2)	0.0090(6)	0.010(1)	

Notes: The measure at room pressure was performed with crystal in air, however, the crystal structure refinement was done after calculating how many Bragg reflections were accessible using the same orientation that the crystal had into the diamond anvil cell.

unit-cell parameters,  $\beta = -1/3K_{T0}$  (for further details see the user guide of EoS-Fit5.2, Angel 2002), also are reported in Table 4. The axial compressibility scheme for pure jadeite (Nestola et al. 2006) is  $\beta_a > \beta_c \approx \beta_b$ , for  $\text{Jd}_{53}\text{Hd}_{47}$  we have  $\beta_b > \beta_a > \beta_c$ , while for  $\text{Jd}_{26}\text{Hd}_{74}$  and  $\text{Jd}_0\text{Hd}_{100}$  the scheme is the same and is  $\beta_b > \beta_c > \beta_a$ . It is therefore evident that an increase of Hd content affects the directions of deformation relative to jadeite. The data in Table 4

demonstrate that  $\beta_a$  remains practically constant along the solid solution, while the linear compressibility along **b** increases by about 35% going from jadeite to hedenbergite. The **c** axis also shows a strong increase in linear compressibility of about 24% with increasing Hd content. The axial compressibility ratio along the solid solution goes from  $\beta_b:\beta_c:\beta_a = 1.15:1.00:1.02$  of jadeite (Nestola et al. 2006) to  $1.05:1.17:1.00$  for  $\text{Jd}_{53}\text{Hd}_{47}$  to

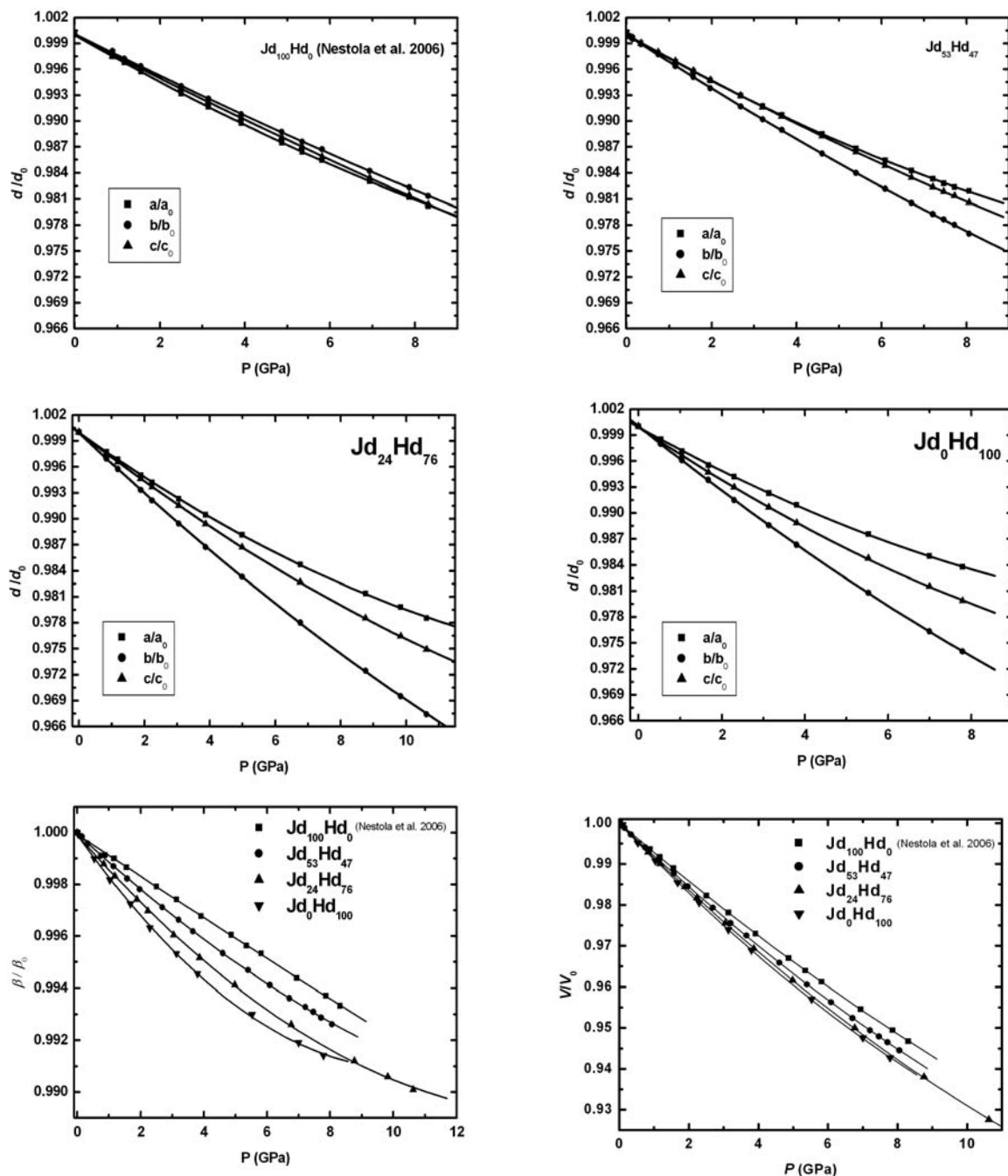


FIGURE 1. Evolution of the unit-cell parameters and volumes with pressure (relative compression) for all samples studied in this work. All data relative to  $\text{Jd}_{100}\text{Hd}_0$  are taken from Nestola et al. (2006). The symbols used in all plots are larger than one standard deviation. Solid curves are the resulting BM3 fits of the data.

1.00:1.28:1.05 for  $\text{Jd}_{24}\text{Hd}_{76}$  and to 1.00:1.34:1.18 for hedenbergite. Thus, increasing the Hd component causes an increase of axial compression anisotropy as also evident in Figure 1.

#### Crystal structure at high pressure

**M2 polyhedron.** The crystal structures of  $\text{Jd}_{100}\text{Hd}_0$ ,  $\text{Jd}_{53}\text{Hd}_{47}$ , and  $\text{Jd}_{24}\text{Hd}_{76}$  were determined up to 8.31, 6.09, and 8.76 GPa, respectively (Table 2 and Table 3), while crystal structure data

for  $\text{Jd}_0\text{Hd}_{100}$  were collected up to 3.80 GPa.

For the purpose of comparison, all the results obtained in this work will be extrapolated assuming as a first approximation a linear behavior to the maximum pressure reached for the sample  $\text{Jd}_{24}\text{Hd}_{76}$ , which was measured up to 8.76 GPa.

The M2 polyhedron along the jadeite-hedenbergite join compresses more than the other polyhedra for all samples investigated. The M2 volume (Fig. 4) decreases by 7.9% in  $\text{Jd}_{100}\text{Hd}_0$ ,

**TABLE 3.** Bond lengths, polyhedral volumes, distortion parameters, and angles for the samples studied in this work

	<b>Jd<sub>100</sub>Hd<sub>0</sub></b>			<b>Jd<sub>53</sub>Hd<sub>47</sub></b>		
	0 GPa*	3.14 GPa	8.31 GPa	0 GPa*	3.65 GPa	6.09 GPa
M2-O1 (Å) ×2	2.365(5)	2.330(6)	2.313(6)	2.374(5)	2.359(10)	2.340(11)
M2-O2 (Å) ×2	2.411(2)	2.389(4)	2.360(5)	2.379(4)	2.370(7)	2.354(8)
M2-O3 (Å) ×2	2.367(3)	2.354(6)	2.352(6)	2.478(6)	2.470(8)	2.452(10)
M2-O3 (Å) ×2	2.748(4)	2.684(6)	2.593(6)	2.740(7)	2.668(8)	2.611(9)
<M2-O>	2.473(10)	2.439(16)	2.404(15)	2.491(10)	2.467(22)	2.442(27)
V (Å <sup>3</sup> ) †	24.762(23)	23.802(26)	22.914(25)	25.458(10)	24.848(42)	24.167(48)
M1-O1 (Å) ×2	1.948(3)	1.930(4)	1.922(4)	2.014(4)	2.009(7)	1.992(8)
M1-O1 (Å) ×2	2.002(5)	1.979(6)	1.948(5)	2.062(5)	2.053(9)	2.029(10)
M1-O2 (Å) ×2	1.862(5)	1.850(6)	1.833(6)	1.970(8)	1.948(9)	1.934(10)
<M1-O>	1.937(10)	1.920(12)	1.901(12)	2.015(9)	2.004(19)	1.987(22)
V (Å <sup>3</sup> )	9.505(12)	9.247(14)	8.991(14)	10.764(13)	10.600(24)	10.330(27)
Quad. elong. ‡	1.0141	1.0140	1.0136	1.0096	1.0082	1.0090
Angle Var. §	44.9502	44.7074	43.4527	31.5208	26.6418	29.1306
T-O1 (Å)	1.616(8)	1.625(6)	1.611(6)	1.623(5)	1.592(8)	1.603(9)
T-O2 (Å)	1.592(3)	1.591(6)	1.584(6)	1.591(5)	1.586(9)	1.584(10)
T-O3 (Å)	1.631(4)	1.626(5)	1.615(5)	1.656(6)	1.638(8)	1.634(9)
T-O3 (Å)	1.640(2)	1.639(5)	1.631(6)	1.662(4)	1.654(8)	1.656(9)
<T-O>	1.620(9)	1.620(10)	1.610(10)	1.633(9)	1.618(15)	1.621(18)
V (Å <sup>3</sup> )	2.163(9)	2.168(6)	2.129(6)	2.218(5)	2.160(10)	2.172(12)
Quad. elong.	1.0055	1.0048	1.0045	1.0054	1.0042	1.0042
Angle Var.	23.6766	20.3164	19.298	22.7419	18.2805	18.1689
O3-O3-O3 (°)	174.7(2)	172.6(5)	169.0(4)	170.2(3)	167.4(7)	165.8(8)
		<b>Jd<sub>24</sub>Hd<sub>76</sub></b>		<b>Jd<sub>0</sub>Hd<sub>100</sub></b>		
	0 GPa*	3.87 GPa	8.76 GPa	0 GPa*	3.80 GPa	
M2-O1 (Å) ×2	2.356(4)	2.336(10)	2.310(16)	2.350(5)	2.334(5)	
M2-O2 (Å) ×2	2.356(4)	2.341(7)	2.328(10)	2.333(4)	2.321(5)	
M2-O3 (Å) ×2	2.549(5)	2.536(9)	2.514(14)	2.623(4)	2.608(5)	
M2-O3 (Å) ×2	2.753(6)	2.648(8)	2.555(12)	2.726(5)	2.633(5)	
<M2-O>	2.505(14)	2.466(23)	2.427(32)	2.509(12)	2.476(13)	
V (Å <sup>3</sup> )	25.944(32)	24.836(30)	23.829(50)	26.049(30)	25.134(26)	
M1-O1 (Å) ×2	2.076(4)	2.083(4)	2.054(7)	2.136(4)	2.125(4)	
M1-O1 (Å) ×2	2.108(4)	2.096(8)	2.066(14)	2.165(5)	2.134(5)	
M1-O2 (Å) ×2	2.029(7)	1.997(6)	1.973(10)	2.090(6)	2.056(5)	
<M1-O>	2.072(12)	2.058(16)	2.032(26)	2.131(11)	2.107(12)	
V (Å <sup>3</sup> )	11.757(17)	11.523(18)	11.088(30)	12.820(18)	12.399(17)	
Elong.	1.0064	1.0059	1.0063	1.0045	1.0040	
Angle Var.	21.0211	18.7169	20.0762	14.9971	13.0163	
T-O1 (Å)	1.626(5)	1.598(4)	1.595(6)	1.602(8)	1.585(5)	
T-O2 (Å)	1.590(5)	1.591(4)	1.592(8)	1.587(4)	1.586(6)	
T-O3 (Å)	1.649(7)	1.658(4)	1.658(6)	1.667(5)	1.663(5)	
T-O3 (Å)	1.672(4)	1.673(4)	1.669(7)	1.688(3)	1.680(5)	
<T-O>	1.635(11)	1.630(11)	1.628(16)	1.636(14)	1.630(10)	
V (Å <sup>3</sup> )	2.228(7)	2.207(7)	2.200(11)	2.230(7)	2.204(7)	
Elong.	1.0051	1.0051	1.0049	1.0060	1.0062	
Angle Var.	21.0895	21.5552	20.6720	24.9599	25.9340	
O3-O3-O3 (°)	167.8(3)	164.6(6)	162.3(9)	164.8(2)	162.4(4)	

\*The measure at room pressure was performed with crystal in air, however, the crystal structure refinement was done after calculating how many Bragg reflections were accessible using the same orientation that the crystal had into the diamond anvil cell.

† Polyhedral volumes, mean bond distances and their standard deviations were calculated using IVTON (Balic-Zunic and Vickovic 1996).

‡ and § calculated as in Robinson et al. (1971).

7.3% in Jd<sub>53</sub>Hd<sub>47</sub>, and 8.1% both in Jd<sub>24</sub>Hd<sub>76</sub> and Jd<sub>0</sub>Hd<sub>100</sub>. Thus, it is evident that there is no significant difference along the jadeite-hedenbergite join within the experimental scatter of the data.

An analysis of the individual M2-O bond lengths shows that M2-O3<sub>(long)</sub> shortens the most, with a decrease in length of 5.9% for pure jadeite, 6.8% for Jd<sub>53</sub>Hd<sub>47</sub>, 7.2% for Jd<sub>24</sub>Hd<sub>76</sub>, and 7.8% for hedenbergite. For the M2-O3<sub>(short)</sub>, the decrease is small compared with M2-O3<sub>(long)</sub> and we observe a shortening by 0.7% for jadeite, 1.5% for Jd<sub>53</sub>Hd<sub>47</sub>, 1.4% for Jd<sub>24</sub>Hd<sub>76</sub>, and 1.3% for hedenbergite. This is consistent with the observation reported by McCarthy et al. (2007). The M2-O3<sub>(long)</sub> bond is classified as a sympathetic bond, in that the rotation of the SiO<sub>4</sub> tetrahedra tends to move O3 toward the M2 site and therefore contribute

to the shortening of the M2-O3<sub>(long)</sub> bond due to compression. The M2-O3<sub>(short)</sub> bond is classified as an anti-sympathetic bond, in that the rotation of the SiO<sub>4</sub> tetrahedra tends to move O3 away from the M2 site, and therefore counteracts the compression of the M2-O3<sub>(short)</sub> bond. The changes in the M2-O2 bond distances display an inverse trend to that of M2-O3, with a decrease in the shortening rate as Hd content increases (from 2.2 to 1.2%). The M2-O1 bond lengths behave like M2-O2, thus decreasing the shortening rate with increasing Hd content from about 2.3% in jadeite to 1.6% in hedenbergite. An important parameter to be analyzed is the distortion parameter ΔM2 (Dal Negro et al. 1982) calculated as M2-O3<sub>(long)</sub> - [(M2-O3<sub>(long)</sub> + M2-O1 + M2-O2)/3]. ΔM2 for jadeite shrinks by about 33.3%, while it

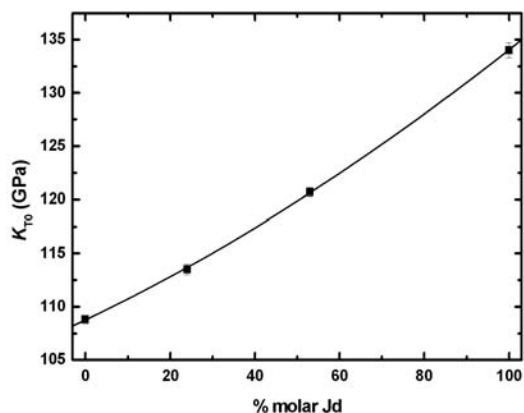


FIGURE 2. Evolution of  $K_{T0}$  as a function of composition along the jadeite-hedenbergite join. The data relative to  $Jd_{100}Hd_0$  are taken from Nestola et al. (2006).

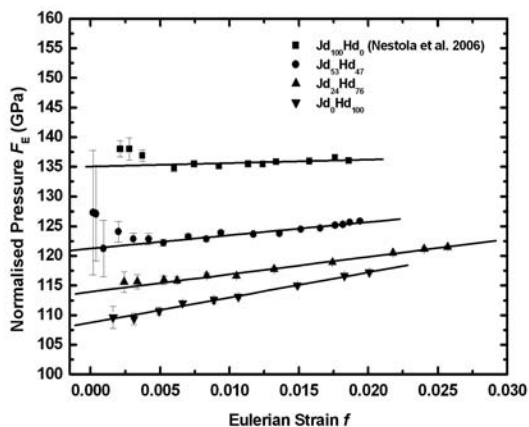


FIGURE 3.  $F_E - f_E$  plot  $\{F_E = P/3 \times f_E \times (1 + 2f_E)^{5/2}$  and  $f_E = [(V_0/V)^{2/3} - 1]/2$ , see Angel 2000} for all samples studied in this work. The data relative to  $Jd_{100}Hd_0$  are taken from Nestola et al. (2006).

decreases by about 44.0% for  $Jd_{53}Hd_{47}$  and 51.4 and 62.6% for  $Jd_{24}Hd_{76}$  and  $Jd_0Hd_{100}$ , respectively. This strong difference in the distortion parameter of the M2 site could explain the small polyhedral volume variation along the join. Although the M2 site of hedenbergite compresses with a similar rate with respect to that of jadeite (and to that of all the other samples along the join), however, it is more regular than that of all the other compositions as it shows 4+4 coordination vs. the 6+2 coordination of jadeite at all pressures.

**M1 octahedron.** M1 octahedral compressibilities vary along the jadeite-hedenbergite solid solution even less than the M2 polyhedral compressibilities. This is illustrated in Figure 5. The M1 volume variations are about 5.7% for all samples with exception of hedenbergite, which decreases about 7.6%. Concerning the M1 distortion parameter (see Table 3), we did not observe any significant trend along the solid solution. The individual M1-O bond distances do not show particular trends: M1-O<sub>(long)</sub> bonds decrease by about 3.2% in pure jadeite and by about 2.5–2.6% from  $Jd_{53}Hd_{47}$  to pure hedenbergite, whereas the M1-O2 bonds decrease by 1.9% in jadeite and by about 3.5 and 3.0% for the intermediate compositions to 2.4% for pure hedenbergite.

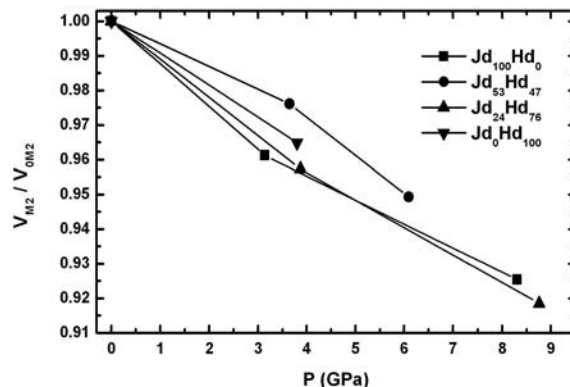


FIGURE 4. Relative compression of the M2 polyhedral volumes along the Jd-Hd join investigated in the present work.

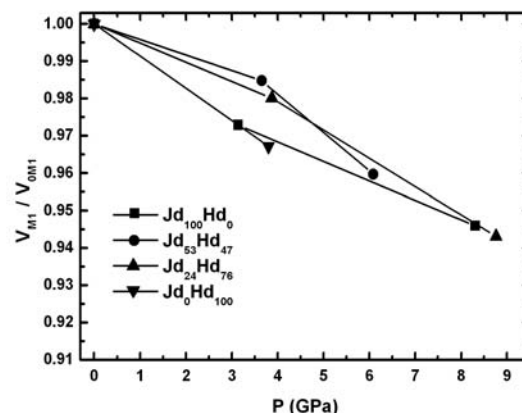


FIGURE 5. Relative compression of the M1 polyhedral volumes along the Jd-Hd join investigated in the present work.

**T tetrahedron.** Tetrahedron behavior with pressure also does not show a well-defined trend in compressibility along the solid solution. The data extrapolated to 8.76 GPa indicate a decrease by 1.6% for the tetrahedral volume of jadeite while the tetrahedral volume of  $Jd_{53}Hd_{47}$  shows a contraction of 2.9%. However, the contraction of the volume is again low for  $Jd_{24}Hd_{76}$  (by about 1.2%) and significantly higher for pure hedenbergite (2.7%). This behavior is consistent with that expected for the strong bonding found in the  $SiO_4$  group.

The tetrahedral chain kinking defined by the O3-O3-O3 angle shows an almost identical contraction rate for all compositions along the join studied in this work. This is also evident in Figure 6, in which the slopes of the linear regressions are practically identical.

**The strain ellipsoid.** The analysis of the unit strain tensor (Ohashi 1982) could clarify the mechanism of structural deformation with pressure along the join. The concept, utility and the calculation procedures of unit strain tensor analysis are discussed in several previous papers (e.g., Origlieri et al. 2003; Nestola et al. 2007; Thompson and Downs 2007). In Table 5, the unit strain ellipsoid size and orientation with pressure along the Jd-Hd join is reported (the data are calculated between 0 GPa and the highest pressure measured for each sample, for

pure Jd the data are taken from Nestola et al. 2006 in which the highest pressure reached for this composition is 8.309 GPa). It is evident that along the join the orientation of the strain ellipsoid with pressure is not constant and the angle between the axis  $\epsilon_3$  and the  $c$  axis decreases from about  $36.8^\circ$  in jadeite to  $30.7^\circ$  in hedenbergite. As a consequence of the monoclinic symmetry displayed by clinopyroxenes, the most compressible directions are along the  $b$  axis and on the (0 1 0) plane. In this work, we observe very strong deformation along  $\epsilon_2$  (coincident with the  $b$  axis) with an increase (in absolute value) by about 48% going from jadeite to hedenbergite, while  $\epsilon_1$  increases by about 34%, and  $\epsilon_3$  shows a smaller decrease by about 7%.

**The  $U_{cp}$  parameter.** Although individual polyhedra compress in a similar way across the jadeite-hedenbergite join, there is a

**TABLE 4.** EoS coefficients for the samples studied in this work

	Jd <sub>100</sub> Hd <sub>0</sub> *	Jd <sub>53</sub> Hd <sub>47</sub>	Jd <sub>24</sub> Hd <sub>76</sub>	Jd <sub>0</sub> Hd <sub>100</sub>
$a_0$ (Å)	9.4279(3)	9.6031(3)	9.7340(2)	9.8847(2)
$K_{a0}$ (GPa)	113.9(8)	114.0(8)	115.2(7)	115.0(8)
$K'$	6.7(2)	9.2(3)	11.2(3)	13.9(4)
$\beta_{a0}$ (GPa <sup>-1</sup> )	-0.00293(2)	-0.00292(5)	-0.00289(2)	-0.00290(2)
$b_0$ (Å)	8.5665(6)	8.7735(3)	8.9103(4)	9.0234(3)
$K_{b0}$ (GPa)	131.4(2.3)	102.8(4)	90.3(2)	85.6(4)
$K'$	3.7(6)	3.5(1)	3.44(5)	3.6(1)
$\beta_{b0}$ (GPa <sup>-1</sup> )	-0.00254(4)	-0.00324(1)	-0.00369(1)	-0.00389(2)
$c_0$ (Å)	5.2262(2)	5.2656(2)	5.2682(2)	5.2509(2)
$K_{c0}$ (GPa)	129.0(3.6)	120.4(4)	109.8(3)	97.7(4)
$K'$	2.8(1.2)	4.4(1)	6.3(1)	9.0(2)
$\beta_{c0}$ (GPa <sup>-1</sup> )	-0.00258(7)	-0.00277(1)	-0.00304(1)	-0.00341(1)
$V_0$ (Å <sup>3</sup> )	402.26(2)	424.90(1)	439.46(2)	450.84(2)
$K_{V0}$ (GPa)	134.0(7)	120.7(4)	113.5(5)	108.8(4)
$K'$	4.4(1)	5.4(1)	5.8(1)	6.6(1)
$\beta_{V0}$ (GPa <sup>-1</sup> )	-0.00746(5)	-0.00828(3)	-0.00881(4)	-0.00919(3)

\* Nestola et al. (2006).  $\beta = -1/3K_0$  for unit-cell parameters and  $-1/K_{V0}$  for unit-cell volumes).

**TABLE 5.** Unit-strain ellipsoid and its orientation calculated with STRAIN (Ohashi 1982) for the different compositions studied in this work

Samples	Strain (GPa <sup>-1</sup> × 10 <sup>2</sup> )			
	$\epsilon_1$	$\epsilon_2$	$\epsilon_3$	$\epsilon_3 \times C$ (°)
Jd <sub>100</sub> Hd <sub>0</sub>	0.1367(7)	0.2245(8)	0.2918(6)	36.8(2)
Jd <sub>53</sub> Hd <sub>47</sub>	0.1201(8)	0.2852(7)	0.2958(5)	34.0(2)
Jd <sub>24</sub> Hd <sub>76</sub>	0.1102(6)	0.3175(5)	0.2953(4)	31.6(4)
Jd <sub>0</sub> Hd <sub>100</sub>	0.1023(8)	0.3336(4)	0.3138(5)	30.7(4)

Notes: Compositions calculated using the unit-cell parameters between 0 GPa and the highest pressure measured for each sample and reported in Table 1; for Jd<sub>100</sub>Hd<sub>0</sub> the data are taken from Nestola et al. (2006) in which the highest pressure for this composition is 8.309 GPa.  $\epsilon_2$  has been chosen as the ellipsoid axis parallel to the  $b$ -axis.

**TABLE 6.**  $U_{cp}$  parameter (Thompson and Downs 2001) at different pressures for the samples studied in this work

	$P$ (GPa)	$U_{cp}$
Jd <sub>100</sub> Hd <sub>0</sub>	0.0001	0.83695
	3.14	0.77880
	8.31	0.69014
Jd <sub>53</sub> Hd <sub>47</sub>	0.0001	0.69408
	3.65	0.62445
	6.09	0.58477
Jd <sub>24</sub> Hd <sub>76</sub>	0.0001	0.59567
	3.87	0.50612
	8.76	0.44204
Jd <sub>0</sub> Hd <sub>100</sub>	0.0001	0.47930
	3.80	0.40258

significant change in the unit-cell compressibility. Thompson and Downs (2001) defined the  $U_{cp}$  parameter and calculated it for several silicates, including clinopyroxenes. This parameter quantifies the distortion of the anion skeleton in a crystal from ideal closest-packing. In some sense, it provides a measure of anion-anion interactions. Small values of  $U_{cp}$  indicate small distortion; 0 is ideally closest-packed while 1 represents a large distortion. The  $U_{cp}$  parameter was calculated for the samples belonging to the Jd-Hd solid solution studied in this work and the results are reported in Table 6. At ambient conditions, jadeite has the highest value of  $U_{cp}$  indicating strong distortion of the anion skeleton from closest-packing, while hedenbergite is much more efficiently packed with an  $U_{cp}$  slightly more than half that of jadeite. Along the join,  $U_{cp}$  shows a non-linear decrease with increasing Hd content. In Figure 7,  $U_{cp}/U_{cp0}$  is plotted against pressure for all the samples along the Jd-Hd join; this figure illustrates that the increase in packing efficiency with pressure is greater with increasing Hd content. If we calculate the decrease of the  $U_{cp}$  parameters to 8.76 GPa, assuming as a first approximation a linear behavior (for purpose of comparison) we determine

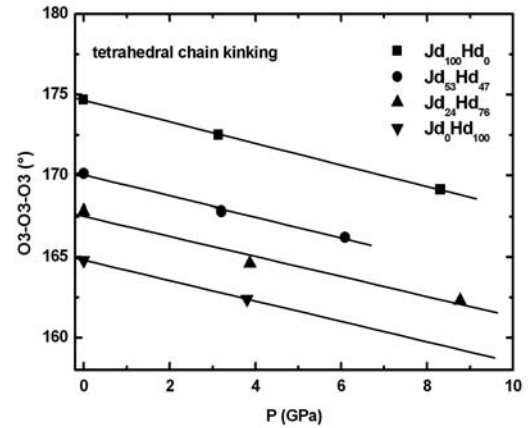


**FIGURE 6.** The tetrahedral chain kinking defined as the O3-O3-O3 angle vs. pressure for the Jd-Hd samples studied in this work.

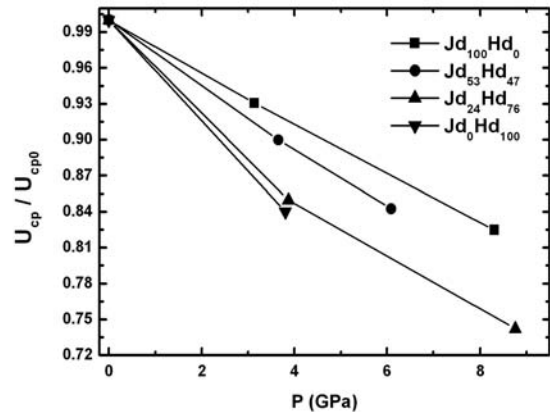


**FIGURE 7.** Observed normalized  $U_{cp}$  parameter (Thompson and Downs 2001) as a function of pressure for the Jd-Hd samples studied in this work.

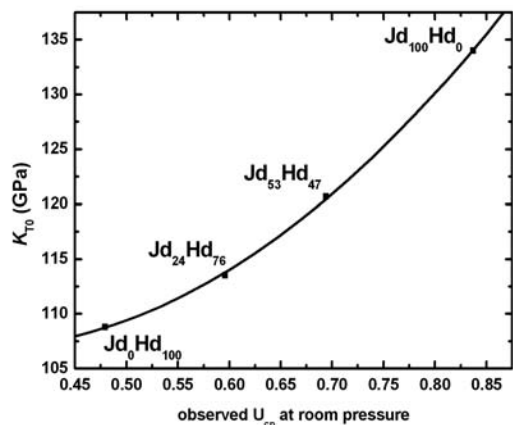


FIGURE 8. Observed  $U_{cp}$  parameter at room pressure (Thompson and Downs 2001) vs. the  $K_{T0}$  (in GPa) determined for the samples studied in this work.

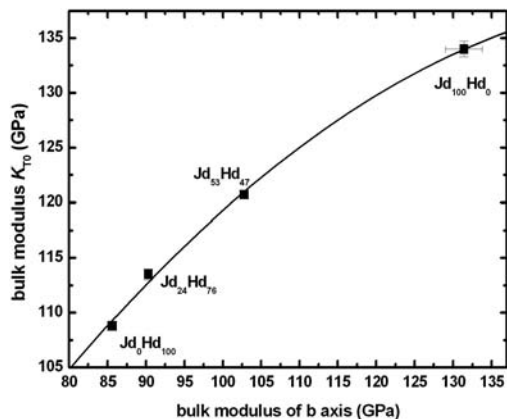


FIGURE 9. The strong correlation between the compressibility along **b** and bulk compressibility along the jadeite-hedenbergite join.

a decrease by 18.5% for jadeite, 22.6% for  $Jd_{53}Hd_{47}$ , 25.8% for  $Jd_{24}Hd_{76}$ , and 36.9% for hedenbergite. This change in the anion skeleton correlates well with the values of bulk modulus (Fig. 8) found along the Jd-Hd join. Therefore, the Hd component of the join goes toward ideal closest packing much more readily than the Jd component and explains the higher compressibility of the Hd-rich compositions.

**M1 chain narrowing.** Figure 9 demonstrates a strong correlation between compressibility along [010] and bulk modulus along the jadeite-hedenbergite join. Thompson and Downs (2007) demonstrated that in diopside almost all of the compression parallel to **b** is the result of the collapse of the M1 chain. The width of the M1 chain can be calculated as  $w_{M1} = (1 - 2y_{O2})b$ . From this, we can calculate the variation of  $w_{M1}$  between room pressure and the maximum pressure reached for all compositions ( $\Delta w_{M1}$ ). Figure 10 shows a good correlation between  $\Delta w_{M1}$  (calculated to 8.76 GPa for purpose of comparison) and the bulk compressibility along the jadeite-hedenbergite join

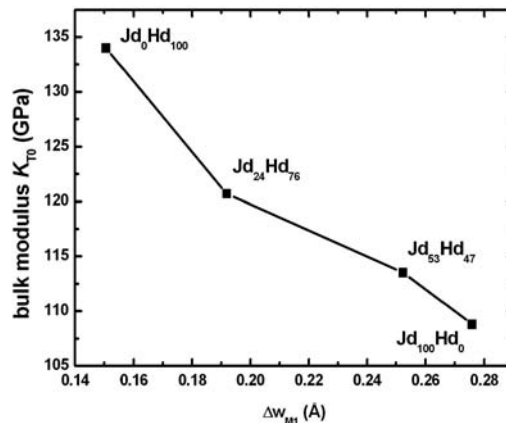


FIGURE 10. The correlation between the narrowing of the M1 chain ( $\Delta w_{M1}$ , see the text) and bulk compressibility along the jadeite-hedenbergite join.

## DISCUSSION

There is a decrease in bulk modulus  $K_{T0}$  with composition along the jadeite-hedenbergite join of about 19%, providing a relation between  $K_{T0}$  and molar fraction of Jd (Fig. 2). Evolution of unit-cell parameters with pressure along the join shows that compressional anisotropy increases with increasing Hd content. In particular, we observed that going from Jd to Hd the compressibility along the **b** direction (the most compressible in pyroxenes) increases by about 35%. However, analysis of crystal structure evolution with pressure along the join shows that there is no significant difference in polyhedral compressibility to justify the decrease of  $K_{T0}$  with increasing Hd content. The M2 site distortion parameter,  $\Delta M2$  (Dal Negro et al. 1982), calculated as a function of pressure for all the samples, decreases more with pressure as Hd content increases. Therefore, the compressibility of the M2 polyhedron is due to a reduction in distortion in addition to simple volume reduction, and this effect becomes more important with increasing Hd content. Another important compression mechanism often proposed for pyroxenes is kinking of the tetrahedral chain (quantified by the O3-O3-O3 angle). In our samples, we observe an identical kinking rate with pressure along the Jd-Hd solid solution (Fig. 6). Therefore, this mechanism does not explain variation in bulk modulus along the join. Thompson and Downs (2007) showed three different compression mechanisms for diopside; among these the authors propose a narrowing of the M1 octahedral chain mainly due to the shift of O2 and M1 atoms parallel to **b**. This mechanism would be the main cause of the compressional anisotropy on the **b-c** plane. A similar behavior is observed for our samples, with O2 showing a larger shift along **b** with increasing Hd content (M1 and O1 atoms showing similar shift rates). The region between the M1 chains displays very little compression in the **b** direction for all samples. The greater collapse of the M1 chain toward its axis as Hd content increases may explain much of the variation in bulk modulus along the join. This collapse is not due to anion-anion interactions, because packing efficiency is maximized when  $y_{O2} = 0.25$ . This is confirmed by the plot in Figure 10, in which the narrowing of the M1 chain strongly increases at high pressure with increasing Hd content.

## ACKNOWLEDGMENTS

F.N. thanks the Alexander von Humboldt for financing this project. Some of the software used to analyze these experiments was developed with National Science Foundation funding through grant no. EAR-9903104, Compression Mechanisms of Upper Mantle Minerals. We thank G.D. Gatta for handling the manuscript, G. Bromiley and an anonymous referee for reviewing and improving this work. This work is part of a wider investigation on jadeite-aegirine-hedenbergite under extreme conditions of pressure and temperature sponsored by the Alexander von Humboldt Foundation.

## REFERENCES CITED

- Allan, D.R., Miletich, R., and Angel, R.J. (1996) A diamond-anvil cell for single-crystal X-ray diffraction studies to pressures in excess of 10 GPa. *Review of Scientific Instruments*, 67, 840–842.
- Angel, R.J. (2000) Equations of State. In R.M. Hazen and R.T. Downs, Eds., *High-Temperature and High-Pressure Crystal Chemistry*, 41, p. 35–39. *Reviews in Mineralogy and Geochemistry*, Mineralogical Society of America, Chantilly, Virginia.
- (2002) EOSFIT V5.2 program. Crystallography Laboratory. Virginia Tech, U.S.A.
- (2003) Automated profile analysis for single-crystal diffraction data. *Journal of Applied Crystallography*, 36, 295–300.
- (2004) Absorption corrections for diamond-anvil cells implemented in the software package Absorb 6.0. *Journal of Applied Crystallography*, 37, 486–492.
- Angel, R.J., Allan, D.R., Miletich, R., and Finger, L.W. (1997) The use of quartz as an internal pressure standard in high pressure crystallography. *Journal of Applied Crystallography*, 30, 461–466.
- Balic-Zunic, T. and Vickovic, I. (1996) IVTON—program for the calculation of geometrical aspects of crystal structures and some chemical applications. *Journal of Applied Crystallography*, 29, 305–306.
- Birch, F. (1947) Finite elastic strain of cubic crystals. *Physical Review*, 71, 809–824.
- Dal Negro, A., Carbonin, S., Molin, G., Cundari, A., and Piccirillo, E.M. (1982) Intracrystalline cation distribution in natural clinopyroxenes of tholeiitic, transitional and alkaline basaltic rocks. In S.K. Saxena, Ed., *Advances in Physical Geochemistry*, p. 117–150. Springer-Verlag, New York.
- Downs, R.T. and Singh, A.K. (2006) Analysis of deviatoric stress from nonhydrostatic pressure on a single crystal in a diamond anvil cell: The case of monoclinic aegirine,  $\text{NaFeSi}_2\text{O}_6$ . *Journal of Physics and Chemistry of Solids*, 67, 1995–2000.
- Holland, T.J.B. (1983) The experimental determination of activities in disordered and short-range ordered jadeitic pyroxenes. *Contributions to Mineralogy and Petrology*, 82, 214–220.
- Hugh-Jones, D.A. and Angel, R.J. (1994) A compressional study of  $\text{MgSiO}_3$  up to 8.5 GPa. *American Mineralogist*, 79, 405–410.
- Hugh-Jones, D.A., Chopelas, A., and Angel, R.J. (1997) Tetrahedral compression in  $(\text{Mg,Fe})\text{SiO}_3$  orthopyroxenes. *Physics and Chemistry of Minerals*, 24, 301–310.
- Ibers, J.A. and Hamilton, W.C. (1974) *International Tables for X-ray Crystallography*, vol. IV. Kynoch, Birmingham, U.K.
- McCarthy, A.C., Downs, R.T., and Thompson, R.M. (2007) In-situ high-pressure single-crystal X-ray study of jadeite, and compressibility trends of clinopyroxenes. *American Mineralogist*, 93, 198–209.
- Nestola, F., Tribaudino, M., and Ballaran, D.B. (2004) High pressure behavior, transformation and crystal structure of synthetic iron-free pigeonite. *American Mineralogist*, 89, 189–196.
- Nestola, F., Ballaran, T.B., Tribaudino, M., and Ohashi, H. (2005) Compressional behavior of  $\text{CaNiSi}_2\text{O}_6$  clinopyroxene: Bulk modulus systematic and cation type in clinopyroxenes. *Physics and Chemistry of Minerals*, 32, 222–227.
- Nestola, F., Boffa Ballaran, T., Liebske, C., Bruno, M., and Tribaudino, M. (2006) High-pressure behavior along the jadeite  $\text{NaAlSi}_2\text{O}_6$ -aegirine  $\text{NaFeSi}_2\text{O}_6$  solid solution up to 10 GPa. *Physics and Chemistry of Minerals*, 33, 417–425.
- Nestola, F., Tribaudino, M., Boffa Ballaran, T., Liebske, C., and Bruno, M. (2007) The crystal structure of pyroxenes along the jadeite-hedenbergite and jadeite-aegirine joins. *American Mineralogist*, 92, 1492–1501.
- Ohashi, Y. (1982) A program to calculate the strain tensor from two sets of unit-cell parameters. In R.M. Hazen and L.W. Finger, Eds., *Comparative Crystal Chemistry*, p. 92–102. Wiley, Chichester.
- Origlieri, M.J., Downs, R.T., Thompson, R.M., Pommier, C.J.S., Denton, M.B., and Harlow, G.E. (2003) High-pressure crystal structure of kosmochlor,  $\text{NaCrSi}_2\text{O}_6$ , and systematics of anisotropic compression in pyroxenes. *American Mineralogist*, 88, 1025–1032.
- Pavese, A., Diella, V., Levy, D., and Hanfland, M. (2001) Synchrotron X-ray powder diffraction study of natural  $P2/n$ -omphacites at high-pressure conditions. *Physics and Chemistry of Minerals*, 28, 9–16.
- Robinson, K., Gibbs, G.V., and Ribbe, P.H. (1971) Quadratic elongation; a quantitative measure of distortion in coordination polyhedra. *Science*, 172, 567–570.
- Sheldrick, G.M. (1997) SHELX, programs for Crystal Structure Analysis. University of Göttingen, Germany.
- Thompson, R.M. and Downs, R.B. (2001) Quantifying distortion from ideal closest-packing in a crystal structure with analysis and application. *Acta Crystallographica B*, 57, 119–127.
- (2004) Model pyroxenes II: Structural variation as a function of tetrahedral rotation. *American Mineralogist*, 89, 614–628.
- (2007) The crystal structure of diopside at pressure to 10 GPa. *American Mineralogist*, 93, 177–186.
- Thompson, R.M., Downs, R.T., and Redhammer, G.J. (2005) Model pyroxenes III: Volume of  $C2/c$  pyroxenes at mantle  $P$ ,  $T$ , and  $X$ . *American Mineralogist*, 90, 1840–1851.
- Tribaudino, M., Prencipe, M., Nestola, F., and Hanfland, M. (2001) A  $P2_1/c$ - $C2/c$  high-pressure phase transition in  $\text{Ca}_{0.5}\text{Mg}_{1.5}\text{Si}_2\text{O}_6$  clinopyroxene. *American Mineralogist*, 86, 807–813.
- Zhang, L., Ahsbahs, H., Hafner, S.S., and Kutoglu, A. (1997) Single-crystal compression and crystal structure of clinopyroxene up to 10 GPa. *American Mineralogist*, 82, 245–258.

MANUSCRIPT RECEIVED AUGUST 30, 2007

MANUSCRIPT ACCEPTED JANUARY 28, 2008

MANUSCRIPT HANDLED BY G. DIEGO GATTA